Supporting Information

A New MXene-derived anthracene-based metal–organic frameworks with controllable morphology for high-performance sensing

*Nasrin Kabeer[a†], Mostafa Zeama[a†], Yusuf khan[b, c], Hadeer Elsayed[b], Jehad K. El-Demellawi[b], Anita Justin[a], Vinayak S. Kale[a], Osama Shekhah[a], Omar F. Mohammed [b], Husam N. Alshareef,[*b,c], and Mohamed Eddaoudi[*a]*

[a] Functional Materials Design, Discovery and Development Research Group (FMD3), Division of Physical Science and Engineering (PSE), King Abdullah University of Science and Technology (KAUST), Thuwal 23955-6900, Kingdom of Saudi Arabia

[b] Center for Renewable Energy and Storage Technologies (CREST), King Abdullah University of Science and Technology, Thuwal, 23955-6900, Saudi Arabia

[c] Materials Science and Engineering, Physical Science and Engineering Division, King Abdullah University of Science and Technology (KAUST), Thuwal, 23955–6900, Saudi Arabia.

Table of Contents

Section S1: Materials and Methods

Powder X-ray diffraction (PXRD) measurements were carried out using a Bruker D8 ADVANCE X-ray diffractometer with Cu Kα radiation (λ = 1.54178 Å). TGA measurements were performed with a TA Instruments Q500 apparatus; the samples were heated under an air atmosphere (flow, 25 cm3.min-1; heating rate, 5 oC/min). Low-pressure gas adsorption measurements were performed at relative pressures of up to 1 atm with a fully automated 3Flex high-resolution gas adsorption analyzer (Micromeritics). The bath temperature for the CO_2 adsorption measurements was controlled with an ethylene glycol/H_2O recirculating bath. Field-emission scanning electron microscope (FE-SEM) images were obtained on a Quattro Dual Beam microscope at an acceleration voltage of 10 kV.

Section S2: Computational details

The electronic structure and adsorption behavior of the MOF system were investigated using density functional theory (DFT) calculations as implemented in the Vienna Ab initio Simulation Package. The projector augmented wave (PAW) method was employed to describe the ion–electron interactions. A plane-wave kinetic energy cutoff of **450 eV** was used throughout all calculations. Exchange–correlation effects were treated using the generalized gradient approximation with the Perdew–Burke–Ernzerhof functional. Brillouin-zone integrations were performed using Monkhorst–Pack scheme k-point meshes, and the electronic occupancies were evaluated using Blöchl tetrahedron method.

The MOF framework structure was first fully relaxed until the forces acting on all atoms were minimized. The optimized structure was subsequently used to analyze the electronic distribution and excited-state charge redistribution within the framework.

To investigate the sensing mechanism toward metal ions, adsorption calculations were performed for **Fe^{3+} and Pb^{2+}** near the vanadium-based metal cluster of the MOF. The $(NO_3)^-$ was used to balance the ion charge. Several initial adsorption configurations were considered to identify the most energetically favorable interaction sites. For each configuration, the atomic positions were fully optimized while maintaining the same computational parameters described above. The optimized structures were then used to determine the preferred adsorption sites, ion–framework distances, and binding energies.

The binding energy of the adsorbed ion was calculated using:

$$E_{bind} = E_{MOF+ion} - (E_{MOF} + E_{ion})$$

Where $E_{MOF+ion}$ is the total energy of the MOF with the adsorbed ion, E_{MOF} is the energy of the isolated MOF structure, and E_{ion} is the energy of the isolated ion. Negative binding energy values indicate favorable adsorption. The optimized geometries were further analyzed to determine the shortest distances between the adsorbed ions and the vanadium-based metal cluster, providing structural insight into the interaction configuration responsible for fluorescence quenching.

Section 3: Material characterization

Figure S1: a) XRD profiles of commercially available V_2AlC MAX phase and etched V_2CTx MXene, (b-c) SEM images of etched V_2CT_X MXene

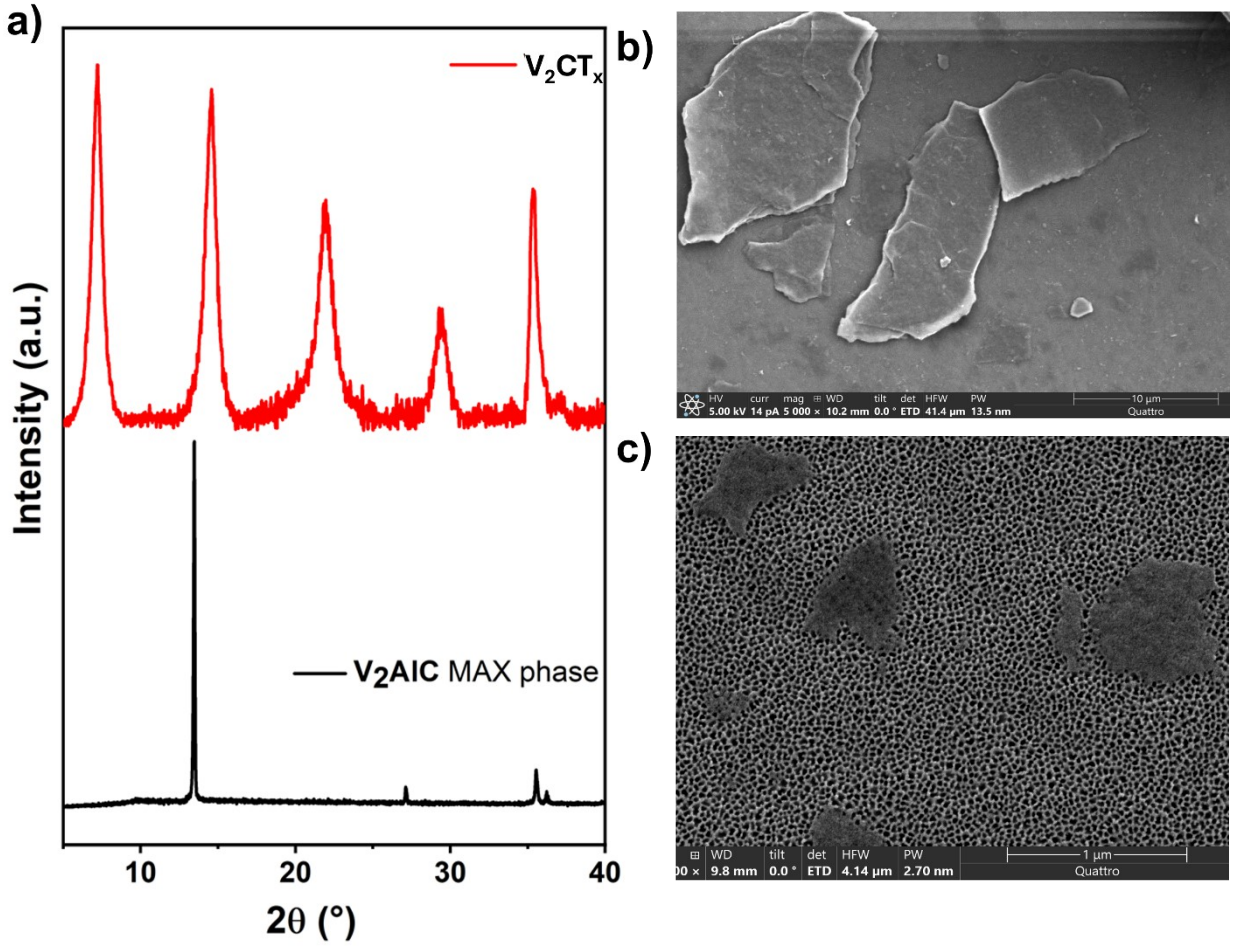

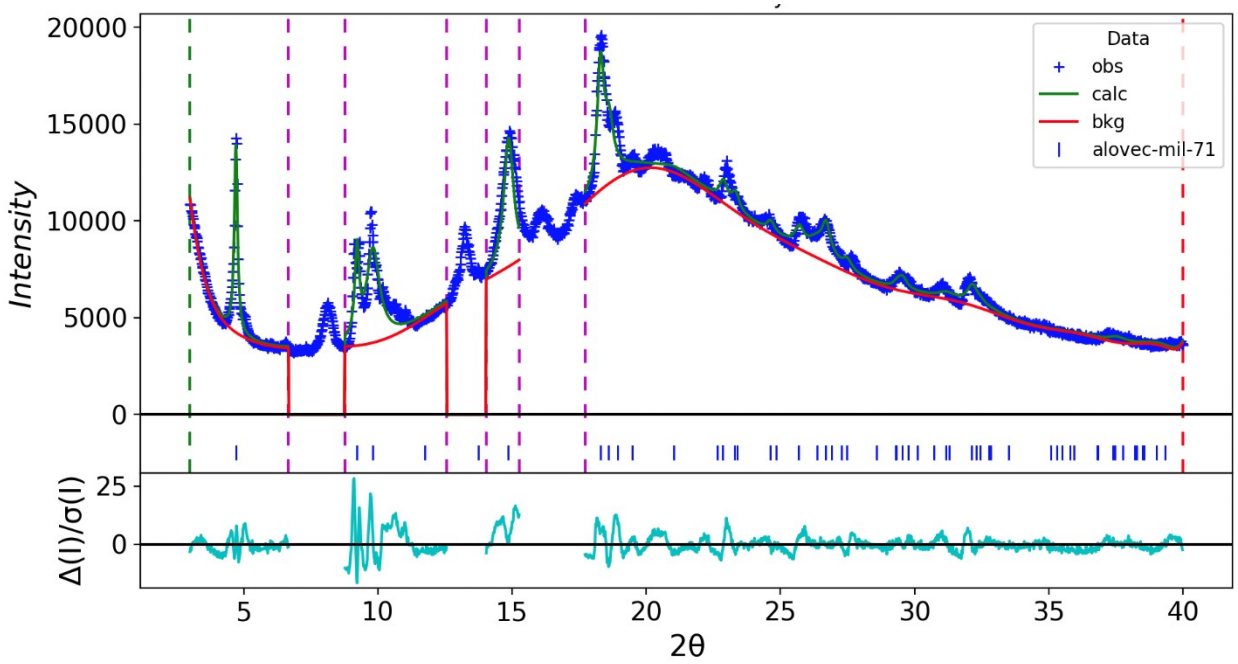

Figure S2: LeBail refinement data

Figure S3: a-b) FT-IR spectra of etched V_2CT_x MXene, V_2CT_x-A MOF, and Ligand

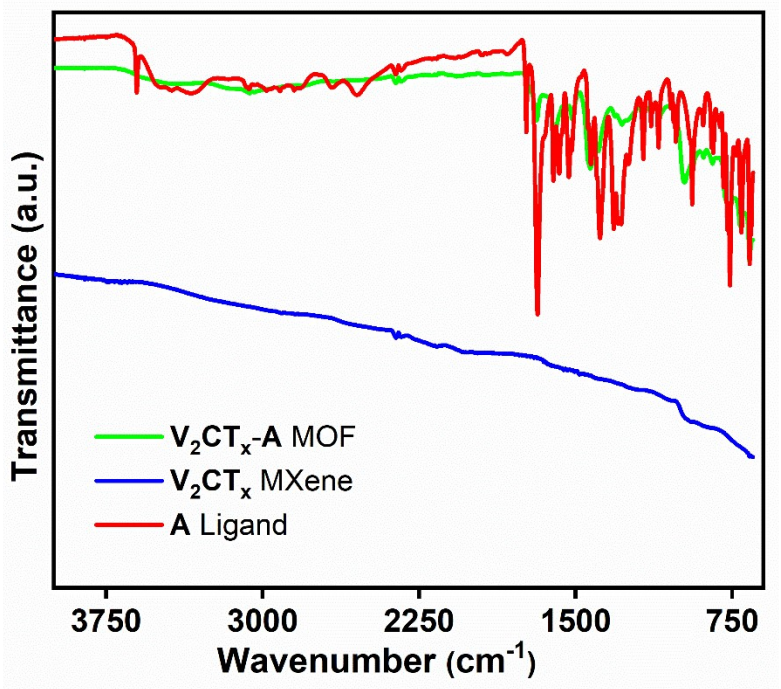

Figure S4: TGA Curves for etched V_2CT_x MXene, V_2CT_x-A MOF, and $VOSO_4$-AMOF

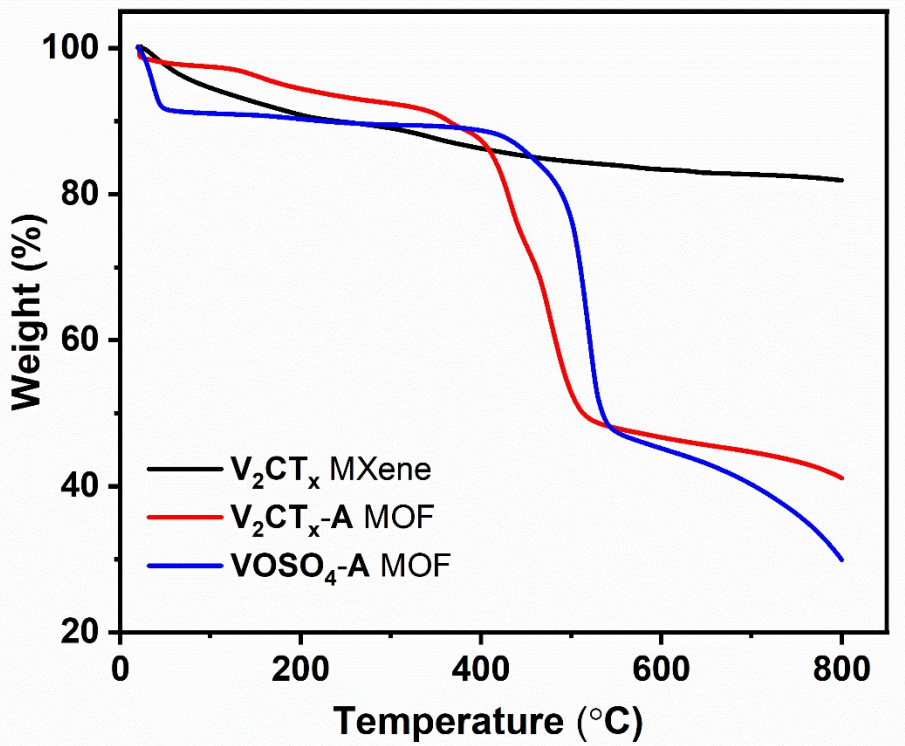

Figure S5: N_2 adsorption-isotherm of $VOSO_4$-AMOF

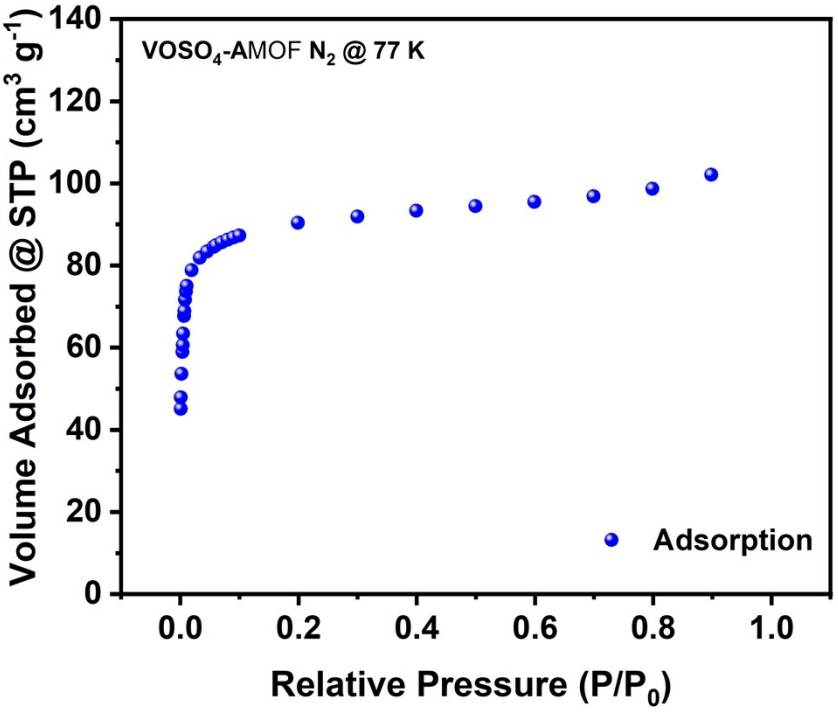

Figure S6: a) N_2 adsorption isotherm, b) Pore size distribution of V_2CT_X-AMOF

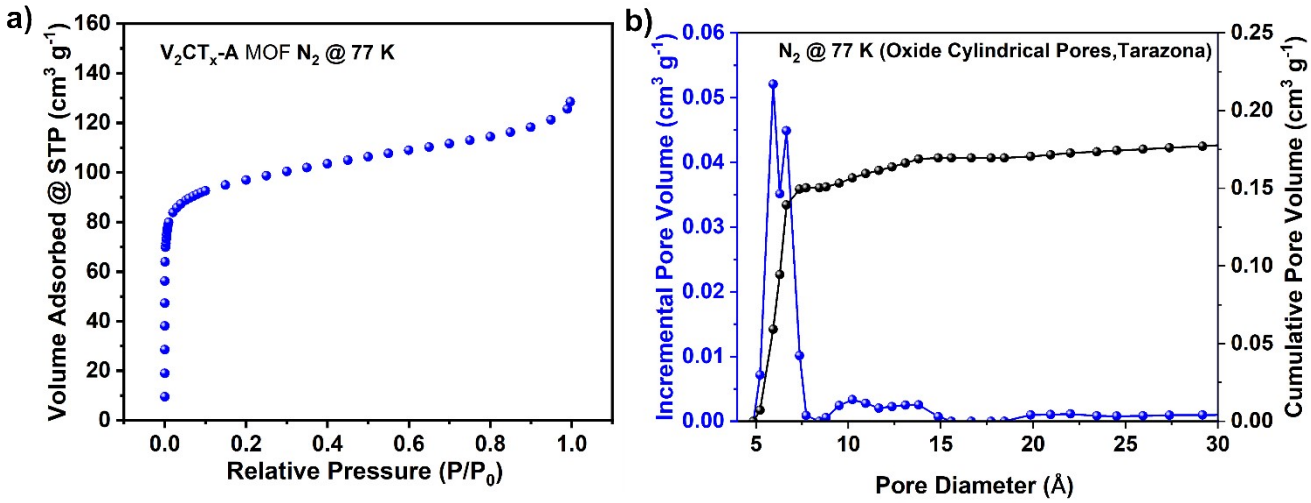

Figure S7: The UV-Vis data for the V_2CT_X-A MOF, and $VOSO_4$-AMOF

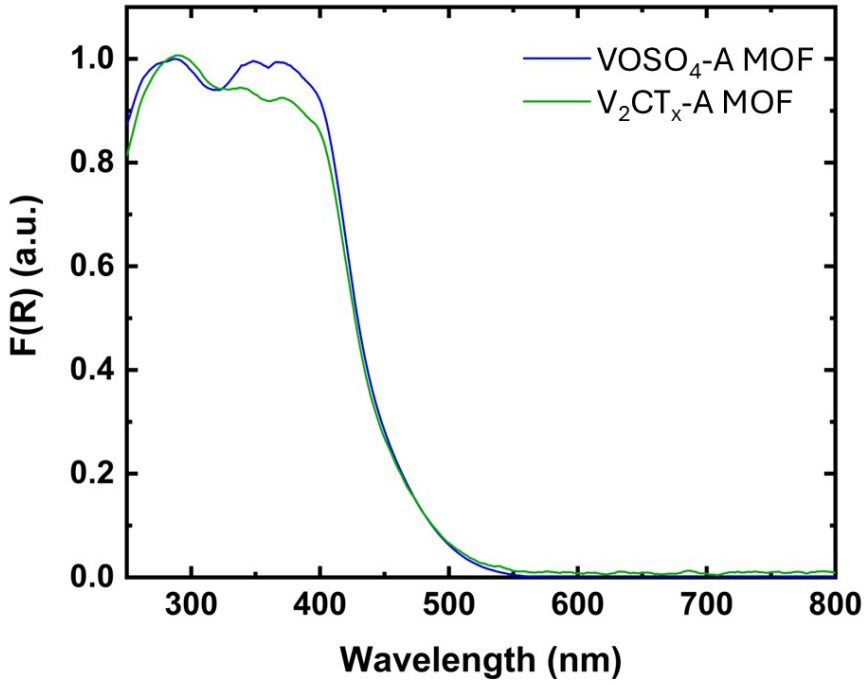

Figure S8: SEM images of a) V_2CT_x-A MOF, b) $VOSO_4$-A MOF

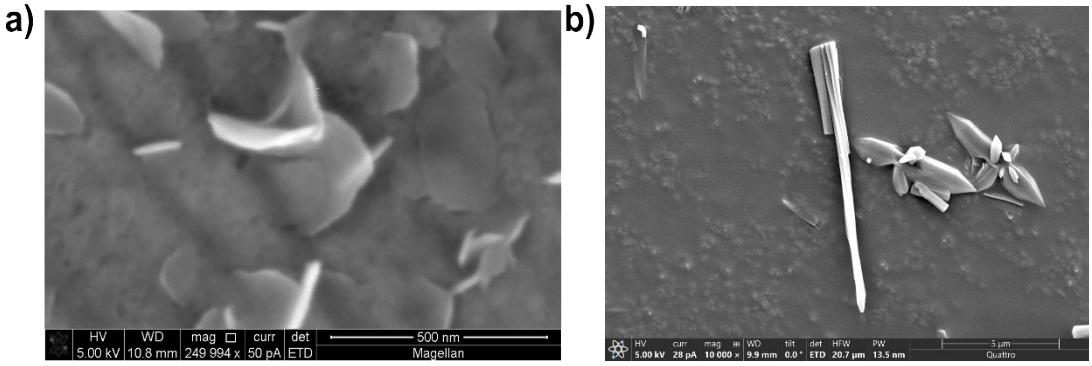

Figure S9: TEM images of a-c) V_2CT_x-A MOF at different magnification

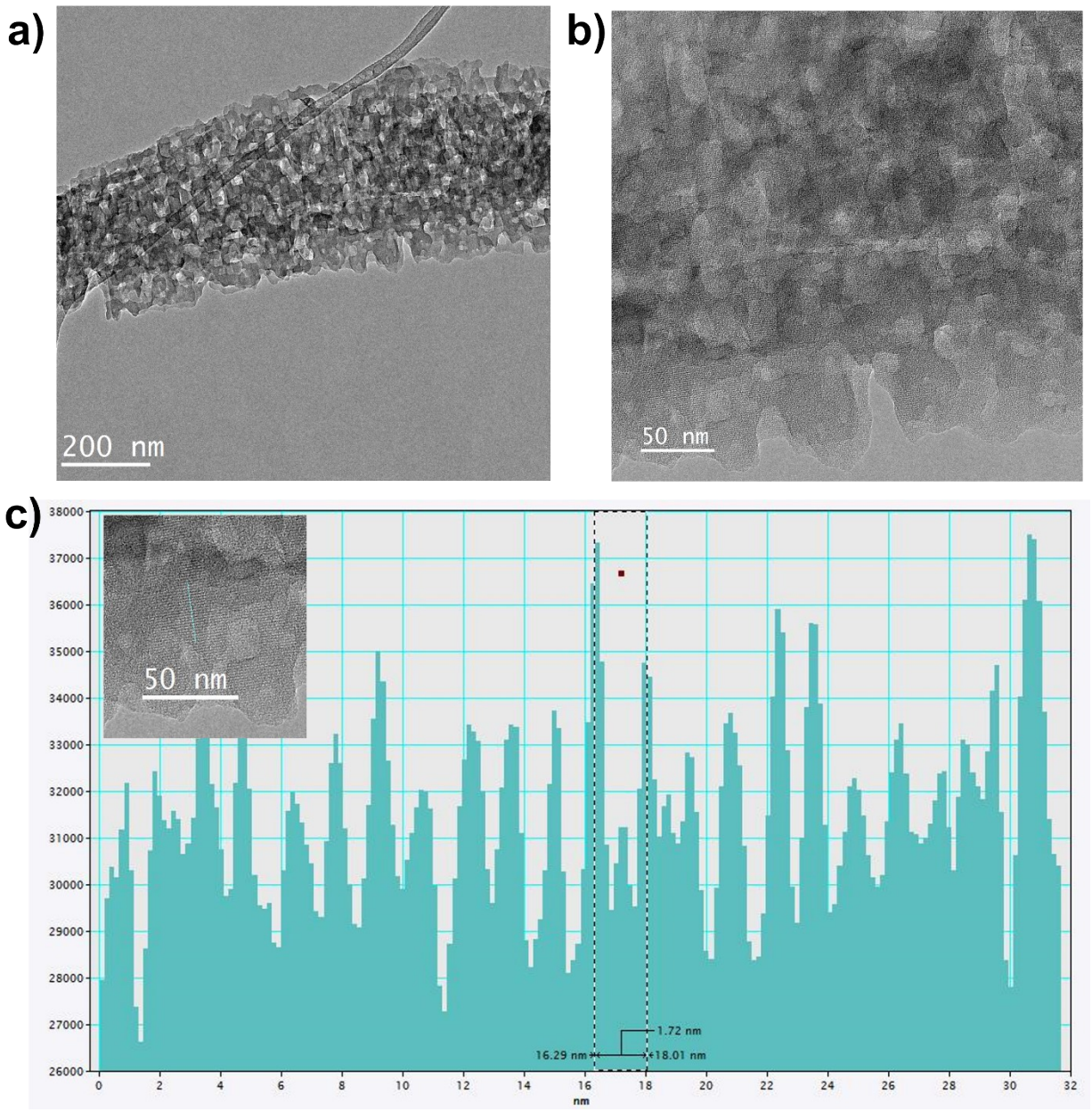
a)
200 nm
b)
50 nm
c)
50 nm
38000
37000
36000
35000
34000
33000
32000
31000
30000
29000
28000
27000
26000
0
2
4
6
8
10
12
14
16
18
20
22
24
26
28
30
32
nm
1.72 nm
16.29 nm
18.01 nm

Figure S10: XPS spectra of V_2CT_x and V_2CT_x-A MOF a-b) survey spectra c) O 1s and V2p d) C 1s.

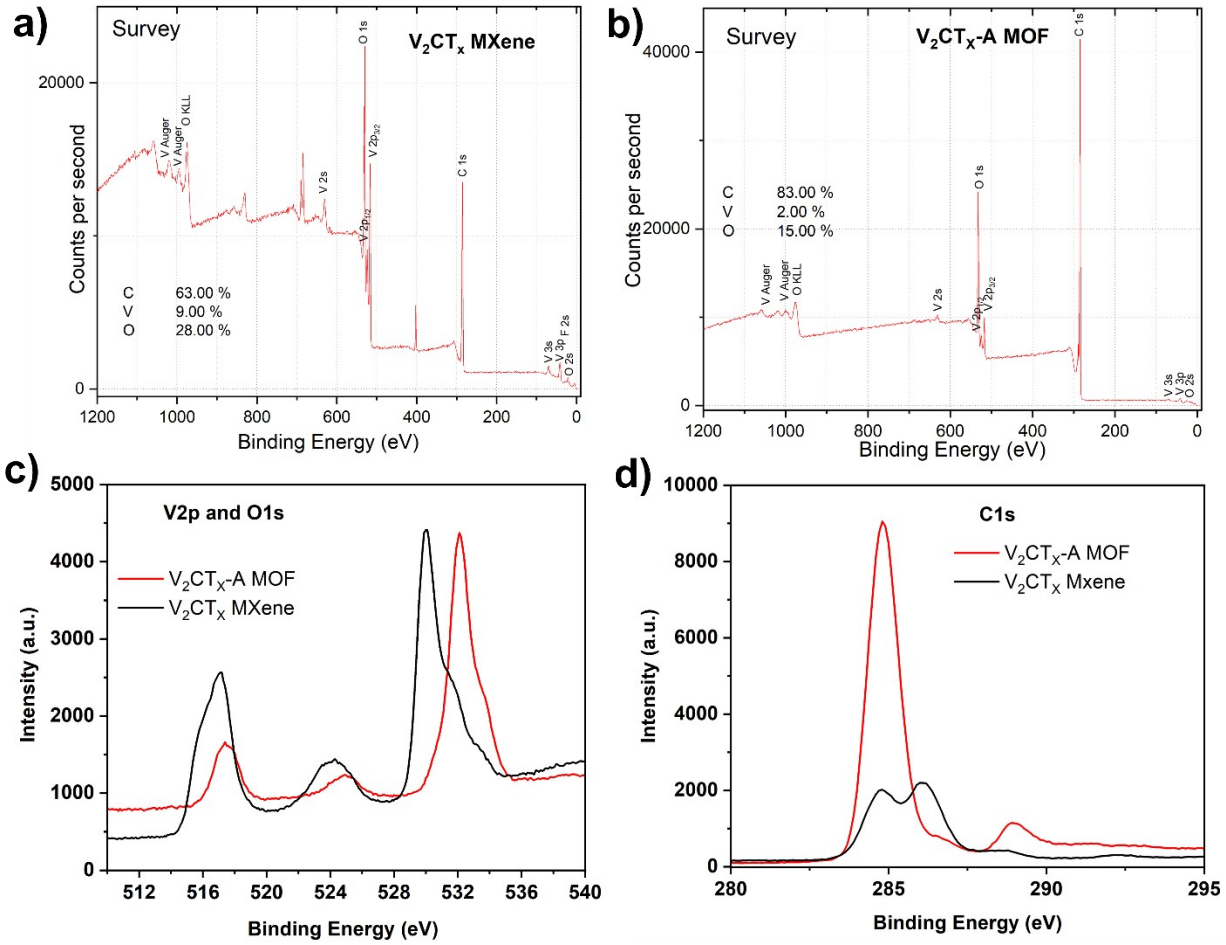

Section S4: Sensing Studies

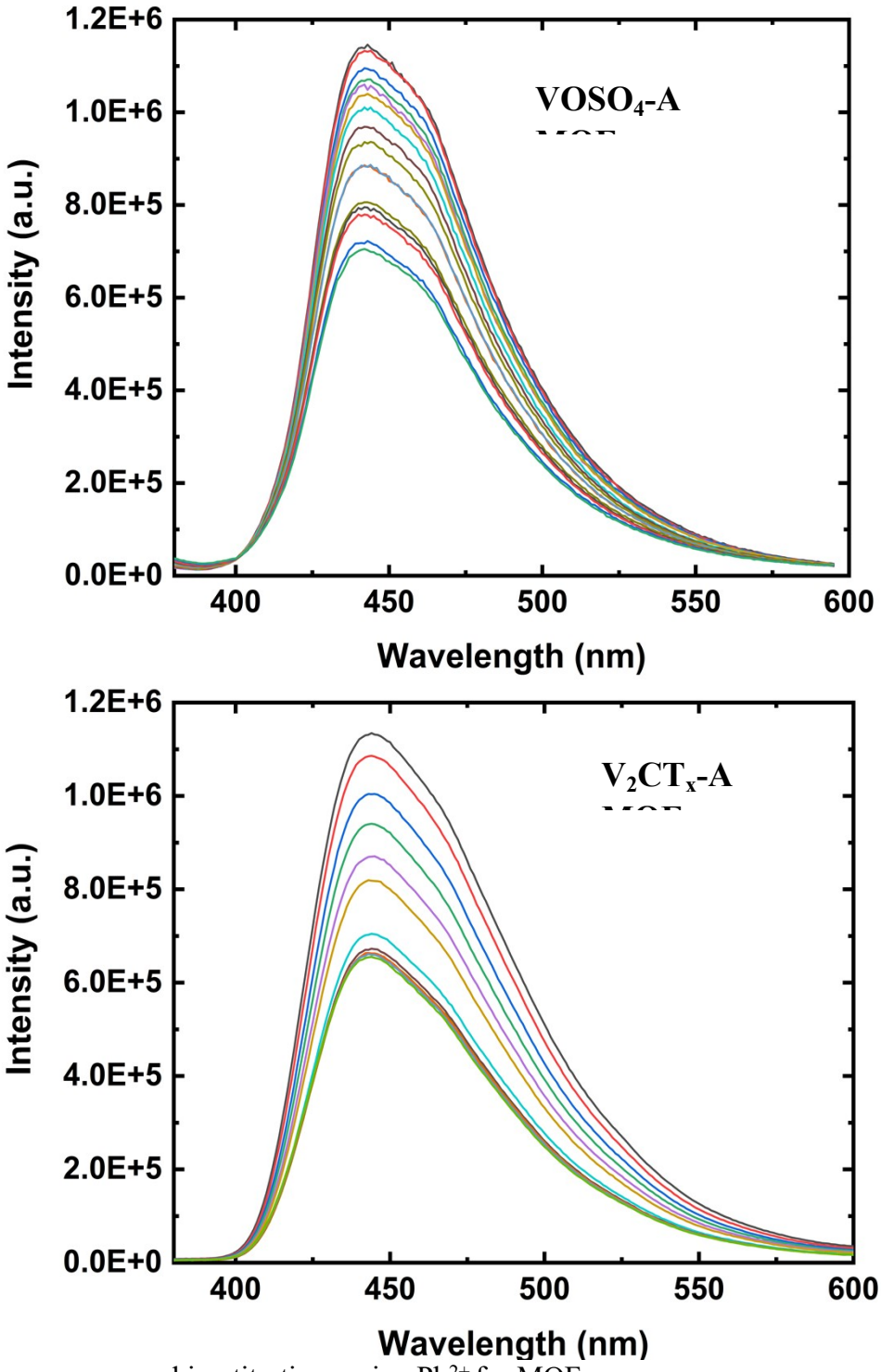

Figure S11: Fluorescence-quenching titrations using Pb^{2+} for MOF

Figure S12: SV plot of $(I_0/I)-1)$ vs. the concentration of Pb^{2+}.

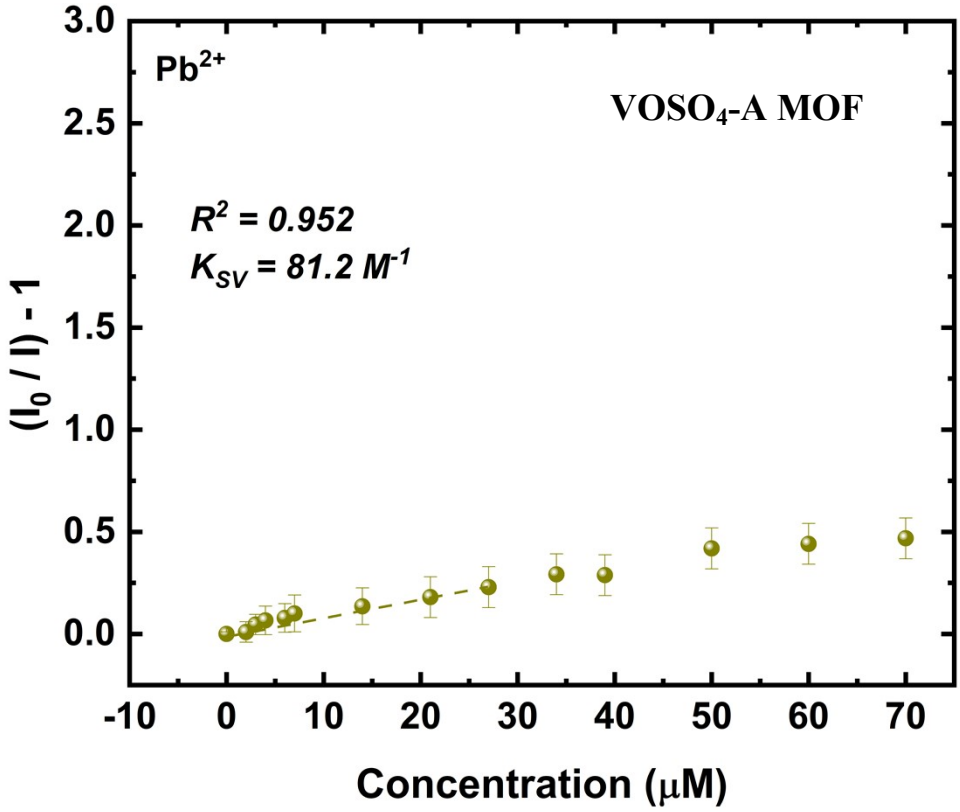

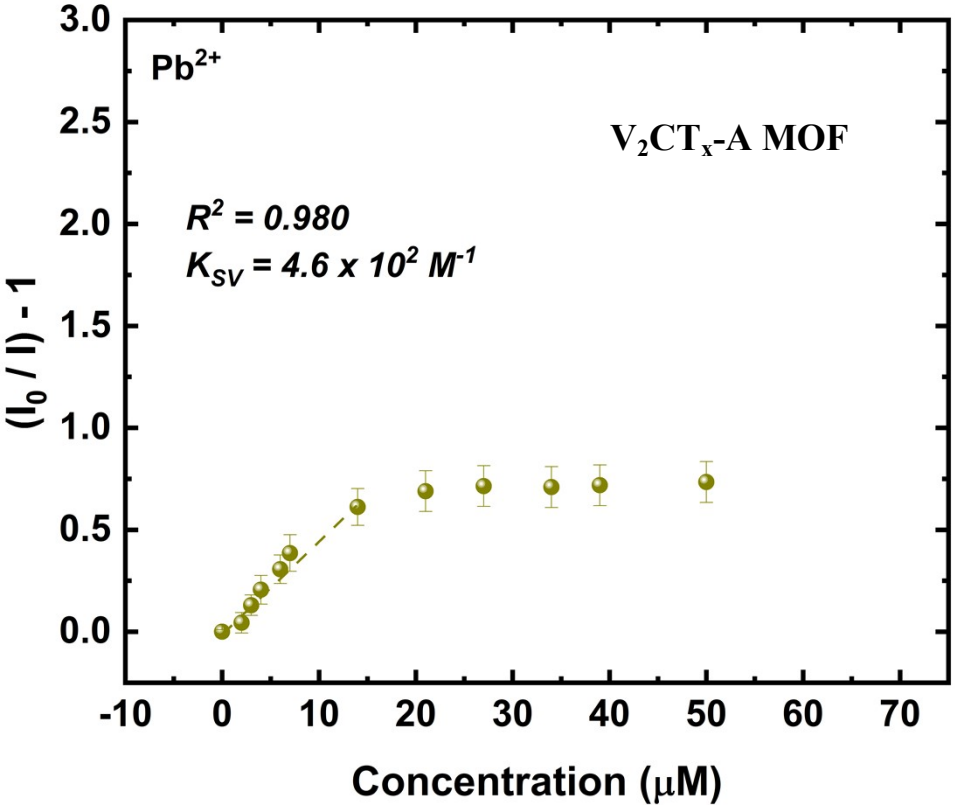

Figure S13: Fluorescence-quenching titrations using Fe^{3+} for MOF in presence of a mixture

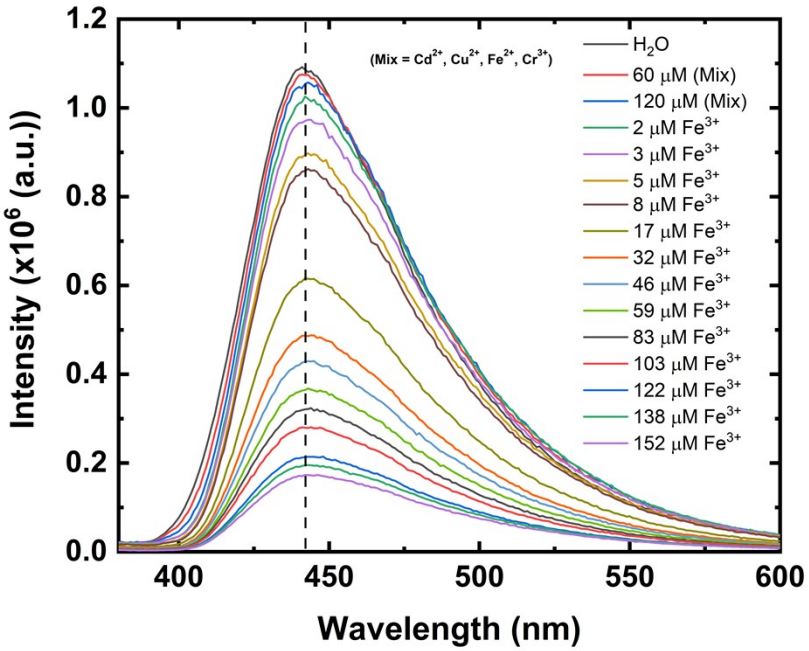

solution

Figure S14: Stability analysis V_2CT_X-A MOF with a) PXRD before and after 24 hours of water exposure, b) PXRD before and after sensing experiment with Fe^{3+}

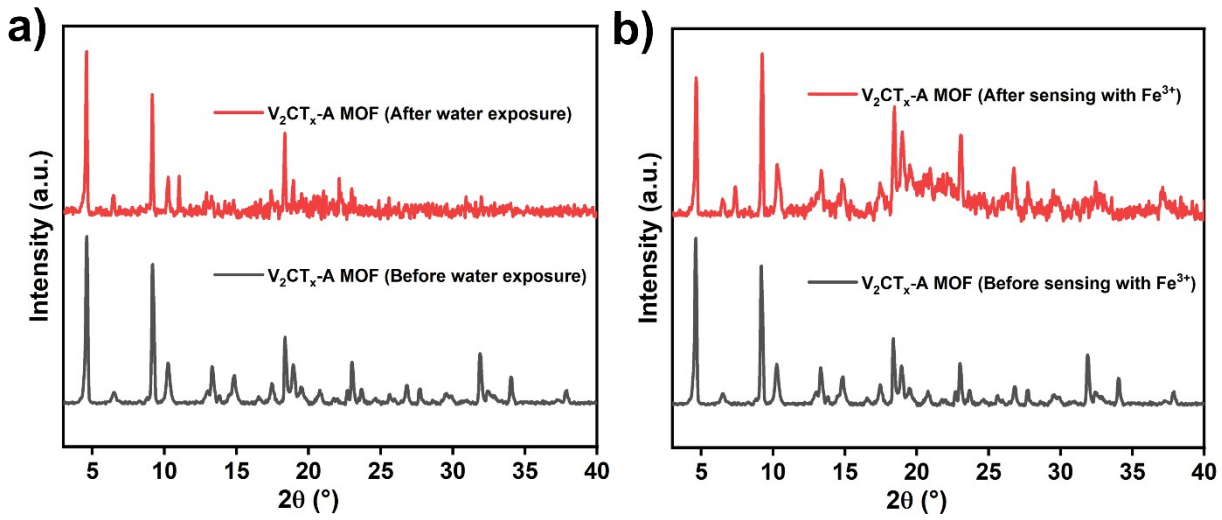

Section S5: Mechanism Studies

Calculation of Spectral Overlap Integral and Förster Distance

To evaluate the possibility of resonance energy transfer between the MOF fluorophore and the analyte species, the spectral overlap integral $J(\lambda)$and the corresponding Förster distance R_0were calculated using the experimentally measured photoluminescence emission spectrum of the MOF and the UV–vis absorption spectra of the analytes.

The spectral overlap integral $J(\lambda)$was determined using the following expression:

$$J(\lambda) = \frac{\int F_D(\lambda)\, \varepsilon_A(\lambda)\, \lambda^4\, d\lambda}{\int F_D(\lambda)\, d\lambda}$$

where

$F_D(\lambda)$is the normalized fluorescence emission spectrum of the donor (MOF), $\varepsilon_A(\lambda)$is the molar absorption coefficient of the acceptor (analyte), and λrepresents the wavelength.

The Förster distance R_0, defined as the donor–acceptor separation at which the energy transfer efficiency is 50%, was calculated using the standard Förster equation:

$$R_0^6 = 8.8 \times 10^{-25}\, \kappa^2\, n^{-4}\, \Phi_D J(\lambda)$$

where

$\kappa^2$is the dipole orientation factor (assumed to be $2/3$for randomly oriented dipoles), $n$is the refractive index of the medium (1.33 for aqueous solution), $\Phi_D$is the fluorescence quantum yield of the donor, and $J(\lambda)$is the spectral overlap integral.

Using the experimentally obtained emission and absorption spectra, the spectral overlap integral was calculated to be:

$$J(\lambda) = 7.85 \times 10^{12}\, M^{-1}\, cm^{-1}\, nm^4$$

Substituting this value into the Förster equation yielded a Förster distance R_0in the range of approximately 2–3 nm, indicating that Förster resonance energy transfer between the MOF fluorophore and the analyte species is geometrically feasible when the analytes are adsorbed near the framework surface. This distance is comparable to the characteristic scale of interactions between the adsorbed ions and the anthracene linkers in the MOF framework, suggesting that resonance energy transfer may contribute partially to the observed fluorescence quenching behavior.

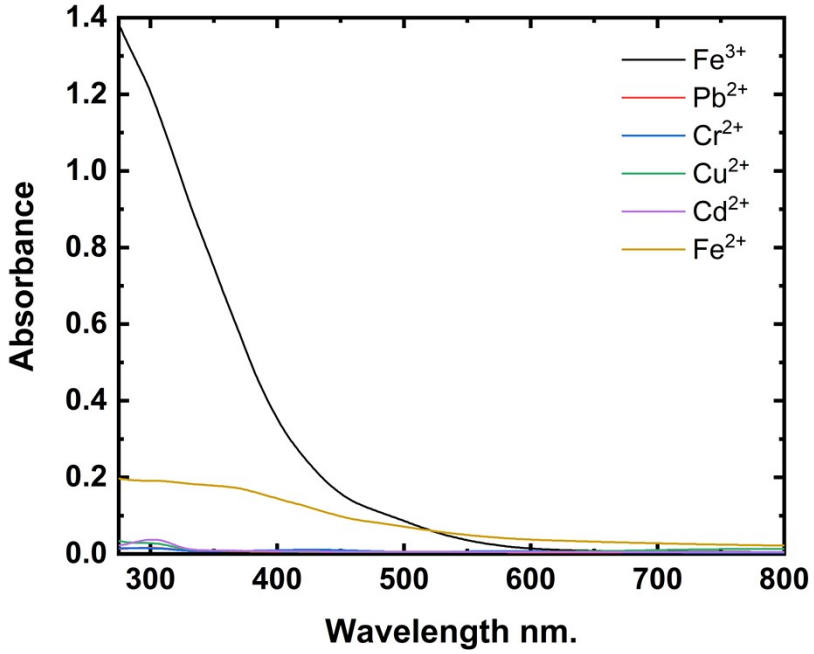

Figure S15: The UV-Vis data for different analytes used in this work

Figure S16: The spectral overlap integral $J(\lambda)$between the MOF emission spectrum and the absorption spectra of the Fe^{3+}

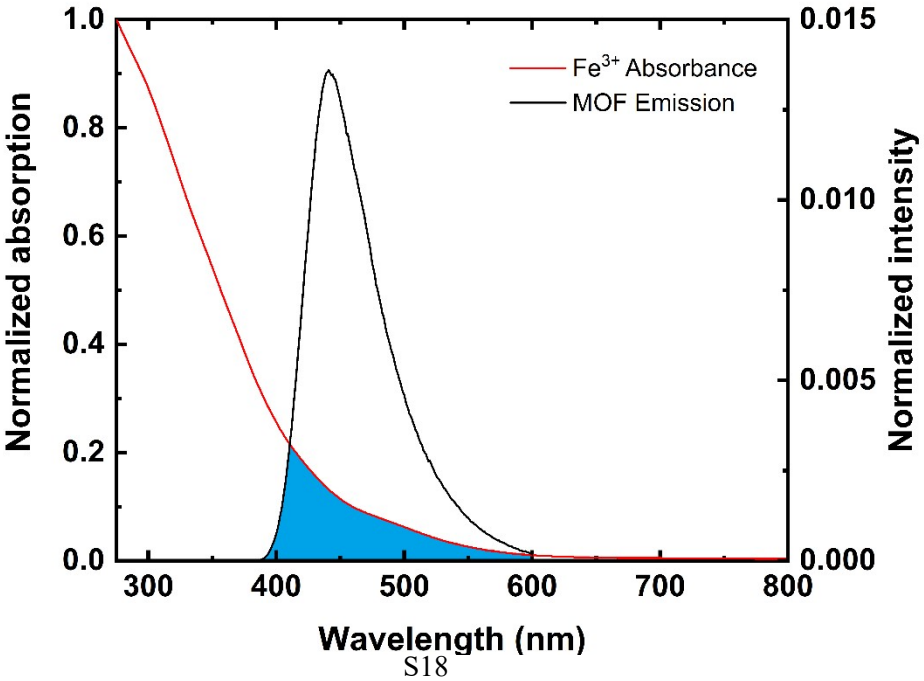

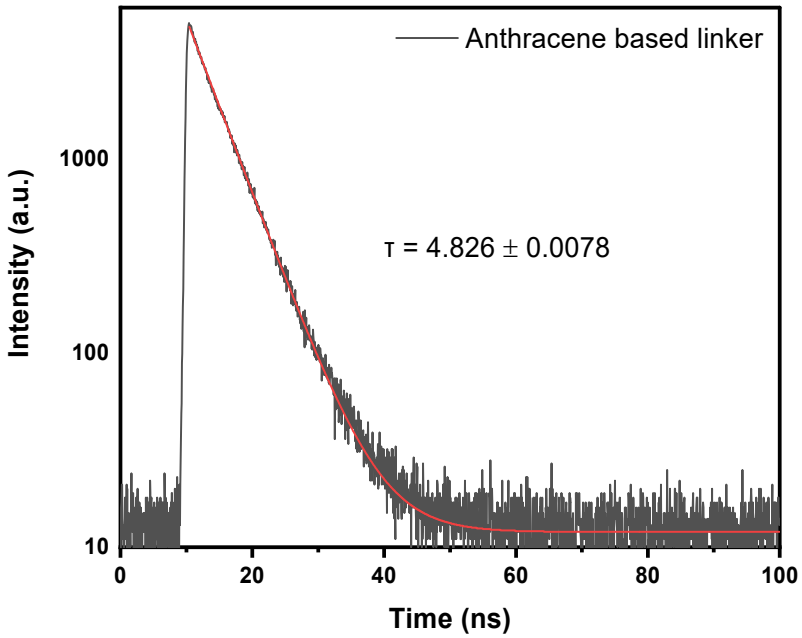

Figure S17: TRPL for the ADBA

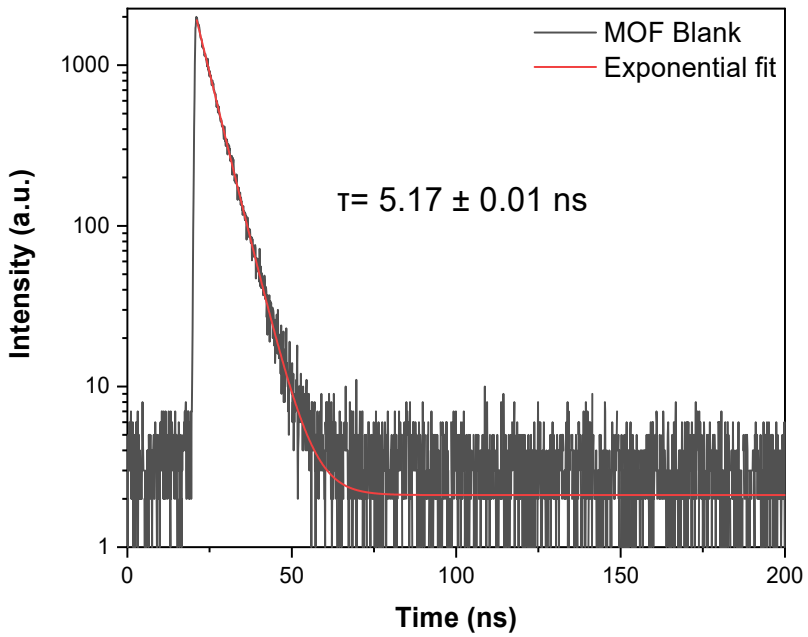

Figure S18: TRPL for the V_2CT_x-A MOF

Figure S19: TRPL for the MOF with Fe^{3+}

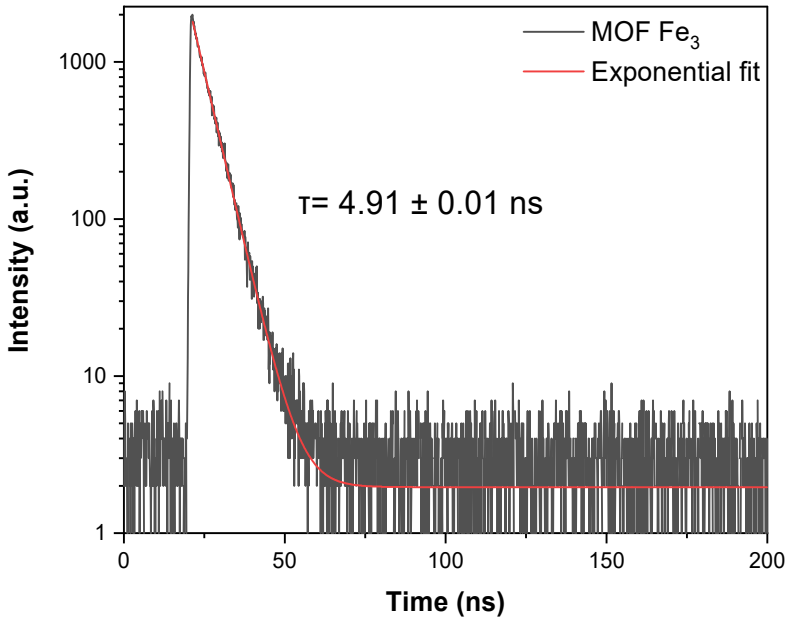

Figure S20: TRPL for the MOF with $Cr_2O_7^{2-}$

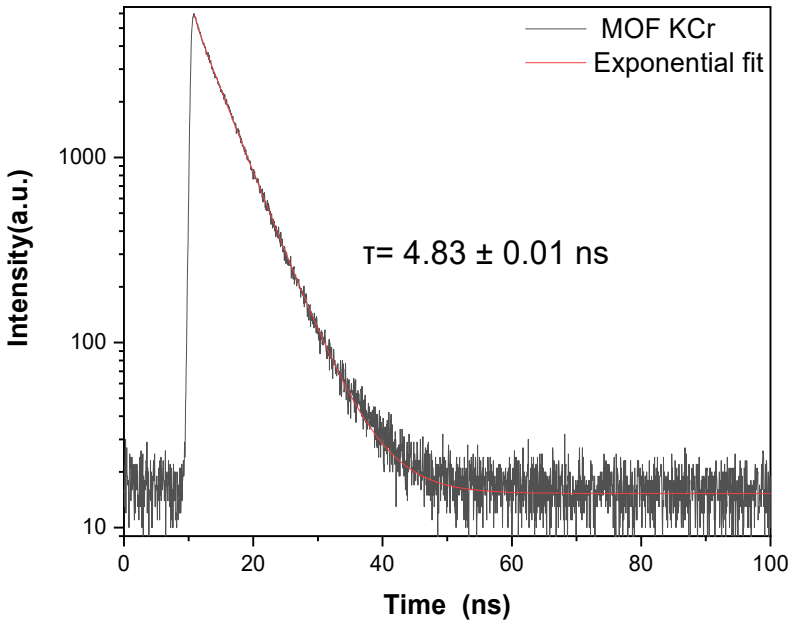

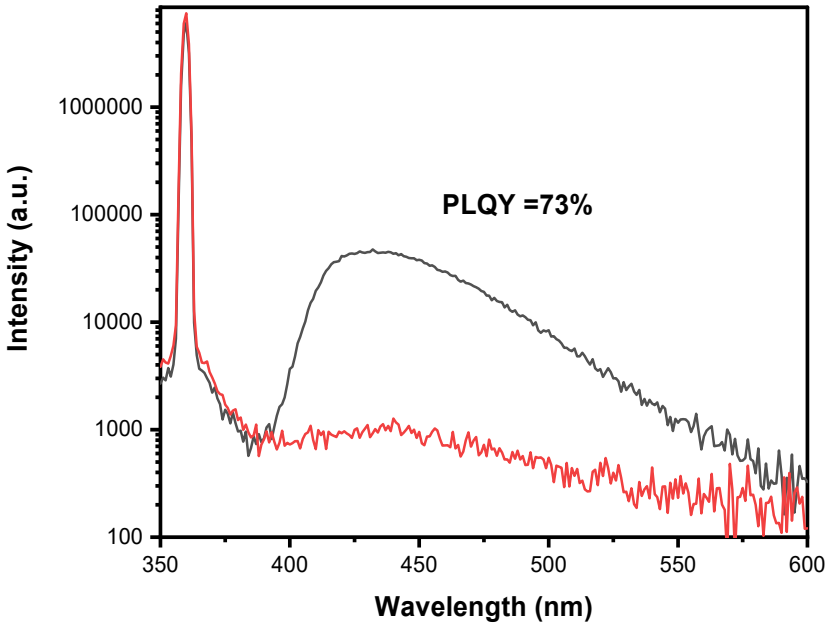

Quantum Yield Results
for 'EmScan5 (QY)'

Scatter Range: 353.00 to 367.00 nm
Emission Range: 383.00 to 600.00 nm

Absorptance : 0.19

QY = 73.01%

Figure S21: PLQY data for V_2CT_X-A MOF

Section S6: Density Functional Theory Calculations

Figure S22: Charge difference between the GS and ES for the MOF. Green clouds indicate excess charge, yellow clouds indicate charge deficiency.

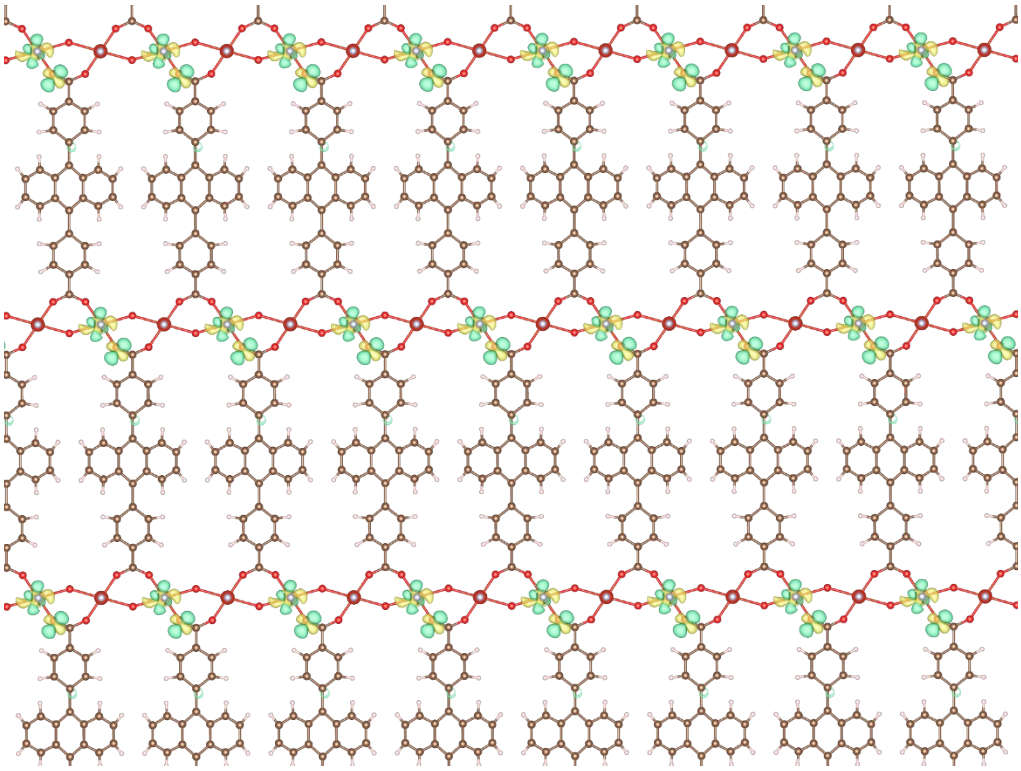

Figure S23: Top view and side view for the adsorption site of Fe^{3+} on the MOF

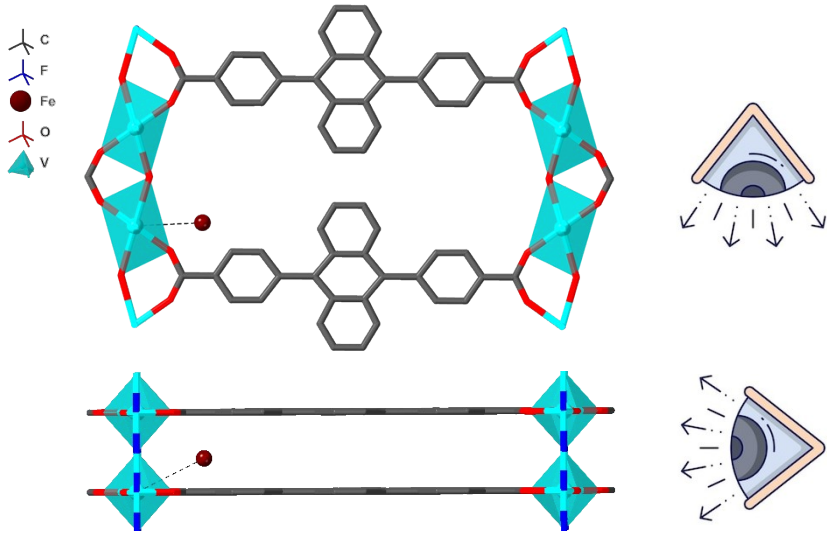

Figure S24: Top view and side view for the adsorption site of Pb^{2+} on the MOF

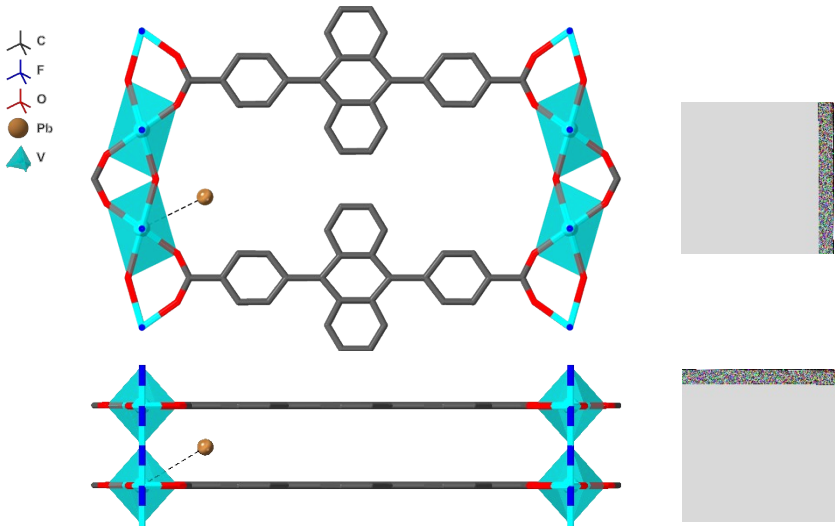

Table S1: distance and binding energy values obtained from DFT calculations

Cation	Distance from V (Å)	Binding energy (eV)
Fe^{3+}	3.4	-11.9
Pb^{3+}	3.8	-3.7